Particle Simulation of Granular Flows in Electrostatic Separation Processes

Ida Critelli

Dipartimento di Ingegneria Meccanica
Politecnico di Milano
Milano, Italy 20126
Email: ida.critelli@polimi.it

Alessandro Tasora

Dipartimento di Ingegneria Industriale
Università di Parma
Parma, Italy 43100
Email: alessandro.tasora@unipr.it

Andrea Degiorgi and
Marcello Colledani

Dipartimento di Ingegneria Meccanica
Politecnico di Milano
Milano, Italy 20126
Email: andrea.degiorgi@polimi.it
Email: marcello.colledani@polimi.it

***Abstract*—In waste processing technology, the recent Corona Electrostatic Separation (CES) method is used to separate conductive from non-conductive particles in recycling streams. This paper proposes an innovative simulation approach based on non-smooth dynamics. In this context, a differential-variational formulation is used to implement a scalable and efficient time integrator that allows the large-scale simulation of trajectories of particles with different properties under the effect of particle-particle interactions and frictional contacts. Issues related to performance optimization, fast collision detection and parallelization of the code are discussed.**

Keywords–Granular flows, particles, waste processing

I. INTRODUCTION

Numerical simulation of waste processing devices is becoming a key factor in the improvement of material recycling: this work focuses on the simulation of the CES processing technology. Such a technology uses electrostatic forces to separate conductor materials from insulating materials within a continuous granular flow.

Particles with a varying degree of materials, such as plastic or copper, are produced by a preprocessing stage where Printed Circuits Boards (PCB) are shred and crushed, then they are dropped on the rotating drum of the ECS device, where corona charging is used to establish a negative charge on particles when passing between two high-voltage electrodes [1].

Research on numerical methods for simulating this class of problems is relatively recent [2][3].

Simulating this type of devices proved to be quite challenging in the past, because it requires the simulation of a so called *dense granular flow*, that is a collection of many particles interacting with the surrounding ones. It is known that only few special cases of granular flows can be simplified into macroscopic models, and in literature there are some example of homogenizations that can lead to simpler Finite Element Analysis (FEA), expecially with spherical particles; but, the case at hand is not one of these. In granular flows each particle, with arbitrary shape and mass properties, exploits three dimensional displacements and rotations, hence six degrees of freedoms are introduced per each particle. If one considers that few seconds of simulation of a waste processing device like our CES can involve hundreds of thousands, if not millions, of particles, this instantly gives an idea of how challenging the problem is from a numerical point of view. On top of this, the fact that particles touch each other, introduces a major complication that cannot be solved with classical tools of ordinary differential equations and that leads to the complex field of non-smooth dynamics.

This motivated our research on a custom software tool that can simulate the CES, and similar separation processes, by means of an efficient solution scheme based on Differential Variational Inequalities (DVI).

Results show that we can obtain reliable simulations with large timesteps and by running a single computer for few minutes. Also, the software tool that we developed can simulate motors, moving parts and other auxiliary devices that might interact with the granular flow.

This article starts with an introductory section about the CES process, then it presents the mathematical background of the DVI simulation algorithm, it discusses how to overcome the difficulty of massive collision detection in granular flows, and finally discusses the computation of electrostatic forces and the software implementation. The last section shows examples of results that can be achieved with this type of simulations.

II. THE ELECTROSTATIC SEPARATION PROCESS

The CES is a waste processing device that separates conductor materials from insulating materials within a granular flow of fine particles. An example, from our labs, is shown in Figure 1.

The granular flow receives a discharge of electricity, which gives high surface charge to the plastic particles, causing them

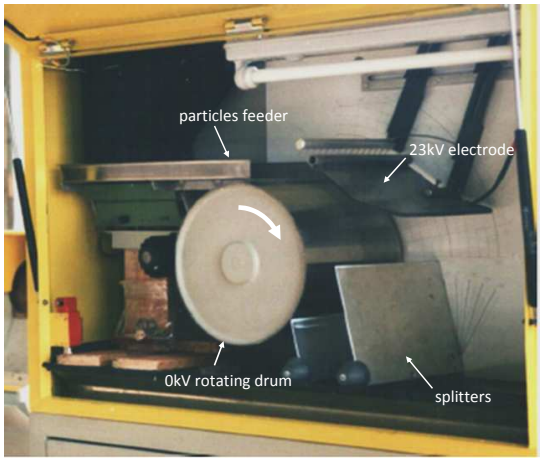

Figure 1: A CES processing device.

 ISBN: 978-1-61208-371-1

to be attracted to the rotor surface until they are brushed down into a proper bin, below the drum. On the other hand, metal particles do not remain charged, because their charge rapidly decreases as they touch the rotor, so they fall into the farthest bin. In case a particle is made of a mixture of materials, it drops in intermediate bins. Metal particles are charged only by electrostatic induction, and this causes a slight attraction effect towards the static electrode of opposite sign.

The efficiency of the process is affected by non-controllable parameters, such as particle shape and size. The quality of the separation can be influenced by controllable parameters like electrode voltage and position, drum speed, splitters position, and feed rate.

III. The DVI formulation

Granular flows are complex dynamical phenomena where a large number of particles interact with each other and with the surrounding environment. The fact that interactions are of discontinuous nature, for example because of hard contacts, introduce a relevant difficulty in the time integration of the system.

Most literature deals with this class of problems by means of the so-called Discrete Element Method (DEM), an approach that regularizes the non-smooth contact phenomena by introducing regularized smooth functions [4]. This means that hard contacts between particles in DEM are approximated as spring-dashpot systems, whose stiff and nonlinear nature requires very short timesteps for the integration of the resulting Ordinary Differential Equations (ODE) [5]. If large timesteps are used in DEM, the explicit ODE time integration may lead to divergence.

In search of a faster and more robust way for simulating granular flows, we developed [6] a time stepping method based on the recent theory of DVI. Such an approach is able to handle up to millions of contacts between particles; it directly captures the discontinuous nature of contacts with set-valued functions, it does not require short integration time steps and it has stability properties that are similar to an implicit method for differential equations.

First researches on a special type of DVI, related to contact problems, can be traced back to the Measure Differential Inclusion theory (MDI) developed in [7][8].

In the DVI framework, the right hand side of a differential expression is a set-valued function [9], so it is an inclusion, as a generalization of classical ODEs that have simple equalities. This is useful in mechanics, since non-smooth pehenomena can be described by means of set-valued functions such as the Signorini contact law or the Coulomb friction. Note that no smooth regularization of discontinuities are needed.

One can discretize DVIs in time, even with large timesteps, obtaining a Variational Inequality (VI) problem for each timestep [10], since reaction forces must satisfy set inclusions rather than algebraic equations.

A DVI is defined as the problem of finding the function $\boldsymbol{x}$ on $[0, T]$:

$$\frac{d\boldsymbol{x}}{dt} = f(t, \boldsymbol{x}, \boldsymbol{u}) \tag{1}$$

$$\boldsymbol{u} \in \mathsf{SOL}\left(\mathbb{K}, F(t, \boldsymbol{x}(t), \cdot)\right) \tag{2}$$

where the state of the system is defined by $\boldsymbol{x}$, and $\mathsf{SOL}(\mathbb{K}, F)$ in the solution of the VI problem:

$$\boldsymbol{u} \in \mathbb{K} \quad : \quad \langle F(\boldsymbol{u}), \boldsymbol{y} - \boldsymbol{u} \rangle \quad \boldsymbol{y} \in \mathbb{K} \tag{3}$$

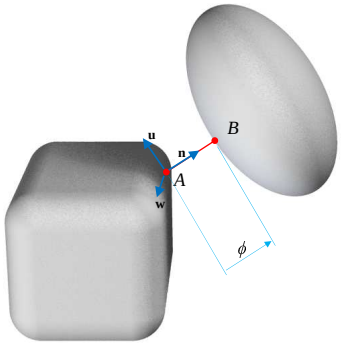

Figure 2: Contact point reference.

given a closed and convex $\mathbb{K} \in \mathbb{R}^n$ set, and given a continuous $F(\boldsymbol{u}) : \mathbb{K} \to \mathbb{R}^n$.

For a problem of particle dynamics, for instance, the state is $\boldsymbol{x} = \{\boldsymbol{q}^T, \boldsymbol{v}^T\}^T$, with positions $\boldsymbol{q}$ and velocities $\boldsymbol{v}$, and $\boldsymbol{u}$ is the set of reaction forces, that must satisfy a VI. For more informations on the DVI theory, see [11]–[15].

In our context of particle dynamics, the granular material is composed of many small particles or large bodies in contact. The system state is defined by the vector of generalized coordinates $\boldsymbol{q} \in \mathbb{R}^{m_q}$ and the vector of generalized speeds $\boldsymbol{v} \in \mathbb{R}^{m_v}$ of the particles. Rotation of each particle is represented with an unit quaternion $\epsilon \in \mathbb{H}_1$ The mass matrix $\boldsymbol{M}(\boldsymbol{q}) \in \mathbb{R}^{m_v \times m_v}$ includes all the masses and inertia tensors of the particles.

Aside from contacts, in granular flow simulations, particles might be affected by field forces such as gravity, aerodynamic forces, etc. In the case of the CES device described here, also forces caused by electrostatic interactions are added. All these forces will be denoted $\boldsymbol{f}_e(\boldsymbol{q}, \boldsymbol{v}, t)$ in the following. The total force field $\boldsymbol{f}_t(\boldsymbol{q}, \boldsymbol{v}, t) \in \mathbb{R}^{m_v}$ includes also the gyroscopic forces $\boldsymbol{f}_c(\boldsymbol{q}, \boldsymbol{v})$; we remark that for the class of problems at hand, gyroscopic forces could be omitted without compromising the results, in search of a more stable numerical integration (because in free falling slender particles, gyroscopic forces often lead to sharp changes in spin directions, thus leading to potential numerical stiffness).

Bilateral constraints are useful to model hinges and joints in devices. In our CES model, for instance, this class of constraints is used to model the revolute joints of the rotating drum, and the constraints for the movable splitting planes. Bilateral joints are introduced via a set $\mathcal{G}_B$ of scalar constraint equations:

$$\Psi^i(\vec{q}, t) = 0, \quad i \in \mathcal{G}_\mathcal{B}. \tag{4}$$

We introduce $\nabla_q \Psi^i = \left[\partial \Psi^i / \partial \vec{q}\right]^T$ and $\nabla \Psi^{i^T} = \nabla_q \Psi^{i^T} \Gamma(\boldsymbol{q})$, to express the constraint (4) at the velocity level after differentiation:

$$\frac{d\Psi^i(\vec{q}, t)}{dt} = \nabla \Psi^{i^T} \boldsymbol{v} + \frac{\partial \Psi^i}{\partial t} = 0, \quad i \in \mathcal{G}_\mathcal{B}. \tag{5}$$

The term $\frac{\partial \Psi^i}{\partial t}$ is needed only for time-dependent constraints. This is the case, in our CES model, of the motor that imposes a constant angular velocity to the rotating drum.

For the i-th contact between two bodies A and B, let $\mathbf{n}_i$ be the normal at the contact point, directed toward the exterior of A, as in Figure 2. Let $\mathbf{u}_i$ and $\mathbf{w}_i$ be two vectors in the contact plane such that $\mathbf{n}_i, \mathbf{u}_i, \mathbf{w}_i \in \mathbb{R}^3$ are orthogonal vectors,

 ISBN: 978-1-61208-371-1

and let Φ_i represent a signed contact distance, assumed to be differentiable at least in vicinity of the contact.

The contact force has a normal component $\boldsymbol{F}_{i,N} = \widehat{\gamma}_{i,n}\mathbf{n}_i$, that must satisfy the Signorini contact rule $\widehat{\gamma}_{i,n} \geq 0 \perp \Phi_i(\cdot) \geq 0$, and a tangential component $\boldsymbol{F}_{i,T} = \widehat{\gamma}_{i,u}\mathbf{u}_i + \widehat{\gamma}_{i,w}\mathbf{w}_i$, caused by friction, along two tangential directions $\mathbf{u}_i, \mathbf{w}_i$, that can represent either the sticking or sliding friction. Within the Amontons-Coulomb theory [16] of dry friction, that we consider adequate for the case of inter-particle friction, the ratio between the normal and the tangential force is limited by friction coefficient μ_i.

Frictional unilateral contacts define a set $\mathcal{G}_A$. For each contact $i \in \mathcal{G}_A$, we introduce the tangent space generators, that can be derived as tangent constraint Jacobians: $\boldsymbol{D}^i_{\gamma_u}$, $\boldsymbol{D}^i_{\gamma_w}$.

We can express the friction model using the maximum dissipation principle, thus leading to a nonlinear program $(\widehat{\gamma}_{i,u}, \widehat{\gamma}_{i,w}) = \operatorname{argmin} \boldsymbol{v}^T (\boldsymbol{D}_{\gamma_u}\widehat{\gamma}_{i,u} + \boldsymbol{D}_{\gamma_w}\widehat{\gamma}_{i,w})$ subject to constraint $\sqrt{\widehat{\gamma}^2_{i,u} + \widehat{\gamma}^2_{i,w}} \leq \mu\widehat{\gamma}_{i,n}$, or equivalently by introducing a multiplier λ_v and writing the Fritz John optimality conditions for such nonlinear program:

$$\nabla_{\gamma_u,\gamma_w}\boldsymbol{v}^T (\boldsymbol{D}_{\gamma_u}\widehat{\gamma}_{i,u} + \boldsymbol{D}_{\gamma_w}\widehat{\gamma}_{i,w}) + -\lambda^i_v \nabla_{\gamma_u,\gamma_w}\left(\mu^i\widehat{\gamma}_{i,n} - \sqrt{\widehat{\gamma}^2_{i,u} + \widehat{\gamma}^2_{i,w}}\right) = 0 \quad (6)$$

$$\mu^i\widehat{\gamma}_{i,n} - \sqrt{\widehat{\gamma}^2_{i,u} + \widehat{\gamma}^2_{i,w}} \geq 0, \quad \perp \quad \lambda^i_v \geq 0. \quad (7)$$

Finally, one can recognize that the following differential model with equilibrium constraints, which expresses the full model of the system including force fields, inertial forces, contacts and bilateral constraints, is a DVI:

$$\begin{aligned}
i \in \mathcal{G}_\mathcal{B} \quad &: \quad \Psi^i(\boldsymbol{q}, t) = 0 \\
i \in \mathcal{G}_\mathcal{A} \quad &: \quad \widehat{\gamma}^i_n \geq 0 \quad \perp \quad \Phi^i(\boldsymbol{q}) \geq 0 \\
&\quad \nabla_{\gamma_u,\gamma_w}\boldsymbol{v}^T (\boldsymbol{D}_{\gamma_u}\widehat{\gamma}_{i,u} + \boldsymbol{D}_{\gamma_w}\widehat{\gamma}_{i,w}) \\
&\quad -\lambda^i_v \nabla_{\gamma_u,\gamma_w}\left(\mu^i\widehat{\gamma}_{i,n} - \sqrt{\widehat{\gamma}^2_{i,u} + \widehat{\gamma}^2_{i,w}}\right) = 0 \\
&\quad \mu^i\widehat{\gamma}_{i,n} - \sqrt{\widehat{\gamma}^2_{i,u} + \widehat{\gamma}^2_{i,w}} \geq 0, \quad \perp \quad \lambda^i_v \geq 0 \\
\dot{\boldsymbol{q}} \quad &= \quad \Gamma(\boldsymbol{q})\boldsymbol{v} \\
\boldsymbol{M}(\boldsymbol{q})\frac{d\boldsymbol{v}}{dt} \quad &= \quad \sum_{i\in\mathcal{G}_\mathcal{A}} \left(\widehat{\gamma}_{i,n}\boldsymbol{D}^i_{\gamma_n} + \widehat{\gamma}_{i,u}\boldsymbol{D}^i_{\gamma_u} + \widehat{\gamma}_{i,w}\boldsymbol{D}^i_{\gamma_w}\right) + \\
&\quad + \sum_{i\in\mathcal{G}_\mathcal{B}} \widehat{\gamma}^i_\mathcal{B}\nabla\Psi^i + \boldsymbol{f}_t(t, \boldsymbol{q}, \boldsymbol{v})
\end{aligned} \quad (8)$$

The DVI model can be discretized in time, using a timestep h. To this end we set $\gamma = h\widehat{\gamma}$, we use an exponential map $\Lambda(\cdot)$ for incremental update of quaternions during the time integration [17][18], and we get:

$$\begin{aligned}
i \in \mathcal{G}_\mathcal{B} \quad &: \quad \frac{1}{h}\Psi^i(\vec{q}^{(l)}) + \nabla\Psi^{i^T}\vec{v}^{(l+1)} + \frac{\partial\Psi^i}{\partial t} = 0 \\
i \in \mathcal{G}_\mathcal{A} \quad &: \quad \gamma_{i,n} \geq 0 \perp \tfrac{1}{h}\Phi^i(\vec{q}^{(l)}) + \nabla\Phi^{i^T}\vec{v}^{(l+1)} \geq 0 \\
&\quad \nabla_{\gamma_u,\gamma_w}\boldsymbol{v}^T (\boldsymbol{D}_{\gamma_u}\gamma_{i,u} + \boldsymbol{D}_{\gamma_w}\gamma_{i,w}) \\
&\quad -\lambda^i_v \nabla \left(\mu^i\gamma_{i,n} - \sqrt{{\gamma_{i,u}}^2 + {\gamma_{i,w}}^2}\right) = 0 \\
&\quad \mu^i\gamma_{i,n} - \sqrt{{\gamma_{i,u}}^2 + {\gamma_{i,w}}^2} \geq 0, \perp \lambda^i_v \geq 0 \\
\boldsymbol{q}^{(l+1)} \quad &= \quad \Lambda(\boldsymbol{q}^{(l)}, \boldsymbol{v}^{(l+1)}, h) \\
\boldsymbol{M}^{(l)}\boldsymbol{v}^{(l+1)} \quad &= \quad \sum_{i\in\mathcal{G}_\mathcal{A}} \left(\gamma_{i,n}\boldsymbol{D}^i_{\gamma_n} + \gamma_{i,u}\boldsymbol{D}^i_{\gamma_u} + \gamma_{i,w}\boldsymbol{D}^i_{\gamma_w}\right) + \\
&\quad + \sum_{i\in\mathcal{G}_\mathcal{B}} \gamma^i_\mathcal{B}\nabla\Psi^i + h\boldsymbol{f}_t(t, \boldsymbol{q}, \boldsymbol{v}) + \boldsymbol{M}^{(l)}\boldsymbol{v}^{(l)}
\end{aligned} \quad (9)$$

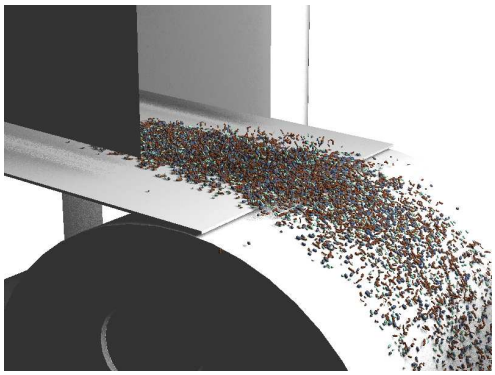

Figure 3: Simulation of the granular flow. Note the different shapes of particles. This example, although simple, leads to half a million of unknown reaction forces in frictional contacts, on average. At each time step, those unknown forces must be solved as a VI problem.

The previous problem is a mixed nonlinear complementarity problem, sub-case of VIs: most results for existence of solutions require monotonicity of the mapping defining the complementarity problem, that also implies convexity of the solution set of the nonlinear complementarity problem [19]. A relaxation of the original problem, that leads to a convex problem whose solution is guaranteed, has been proposed in [20] and it is used in our software.

Once cast to a convex problem, this can be formulated as a second-order Cone Complementarity Problem (CCP), that is also a special type of VI and is also a conically-constrained quadratic optimization problem. As a convex optimization problem, it can be solved by a modification of the Spectral Projected Gradient (SPG) method for the solution of convex-constrained optimization problems, developed by [21]. In the original SPG scheme, the projection operator performs the projection on boxed constraints, whereas we perform projection on the friction cones.

The formulation of (9) can describe only inelastic collisions; but a simple modification can also introduce a restitution coefficient.

We remark that the contact model is based on few parameters (friction coefficient, optionally also restitution coefficient or compliance and damping). Although limited in number of parameters, this simplicity pays back in terms of high computational efficiency and ease of use.

IV. Collision detection

One of the biggest bottlenecks in granular flow simulations is the computation of the collision points between pairs of particles, and between particles and the surrounding environment. There are two main sources of difficulties: one is related to finding the pairs of potential contacting bodies, and the other is computing the geometric location of the contact point(s) between those pairs.

The first difficulty is addressed by the so-called *broadphase* collision detection stage. Such algorithm consists in prefiltering the particles in order to detect only the small portion of pairs that potentially could collide, hence avoiding a brute force $O(n^2)$ test for all pairs - clearly inpracticable even for few thousands of particles. Our broadphase stage leverages the Bullet3D open-source library [22].

 ISBN: 978-1-61208-371-1

The second difficulty is related to the fact that there are many types of collision shapes, as shown in Figure 3, and contact points must be created for pairs in this second phase, called *narrow phase*. Ideally on would like to use polihedrons, spheres, cylinders, boxes etc., as well as compounds of those primitives, but then, algorithms for all possible combination between those types must be implemented. A solution could be to use algorithms of the GJK family [23] that requires only a single member function for each class of primitive, i.e., the computation of the support point. This is the default narrow-phase algorithm for the Bullet3D library, however we experienced that the GJK algorithm suffers a noticeable lack of precision when working with primitives whose size is largely different, which is exactly the case of the small particles that come into touch with the rotating cylinder. To overcome this problem, we implemented a closed form solution for computing contacts between spheres and cylinders (interesting enough, GJK is not affected by this issue for the sphere-vs-box case). This works properly; but if one desires particles that are non-spherical, for instance conical, this would require the development of other closed form algorithms for cone-vs-cylinder, cone-vs-cone, etc. To avoid this increase in coding complexity, and yet resolve the issue of low precision in GJK, we decided to model the collision shape of irregular particles by using cluster of spheres, as in Figure 4. This is an approximation of the real shapes (which are known only at a statistical level anyway), but it performs well in terms of algorithmic robustness and precision.

The ability of simulating particles with non-spherical shapes is important because, as discussed by Lu et al. [3], the shape of the particle can affect the global outcome of the separation process; for example, spherical particles tend to fall farther than thin and slender particles.

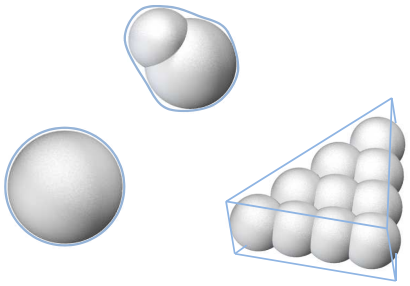

Figure 4: Concept of spherical decomposition.

We experienced that the idea of using cluster of spheres as collision shapes can fit well into parallel computing architectures of the Grpahical Processing Unit (GPU) type, as shown in [24].

V. FORCES FIELDS

At each simulation timestep, the force fields acting on each particle must be updated.

In this model, forces are different for metal and non-metal particles [1]. In case of metals, for the j-th particle, forces acting on the particle are: electric force $\boldsymbol{f}_{el,j}$, aerodynamic drag force $\boldsymbol{f}_{a,j}$ and gravity force $\boldsymbol{f}_{g,j}$, plus it can be affected to the contact forces described in the previous paragraphs. Hence, in the DVI of (8), one has:

$$\boldsymbol{f}_{t,j}(\boldsymbol{q}, \boldsymbol{v}, t) = \boldsymbol{f}_{c,j} + \boldsymbol{f}_{el,j} + \boldsymbol{f}_{a,j} + \boldsymbol{f}_{g,j}$$

On the other hand, forces acting on particles made of non-metal materials are: electric image force $\boldsymbol{f}_{im,j}$, aerodynamic drag force $\boldsymbol{f}_{a,j}$, and gravity force $\boldsymbol{f}_{g,j}$, plus the contact forces if any. In this case it holds:

$$\boldsymbol{f}_{t,j}(\boldsymbol{q}, \boldsymbol{v}, t) = \boldsymbol{f}_{c,j} + \boldsymbol{f}_{im,j} + \boldsymbol{f}_{a,j} + \boldsymbol{f}_{g,j}$$

An analytical model has been used for computing the electric field $\boldsymbol{E}(x, y, z)$ in the space between the two electrodes; to this end we used the formulas expressed in [2]. The resulting electric field is depicted in Figure 5.

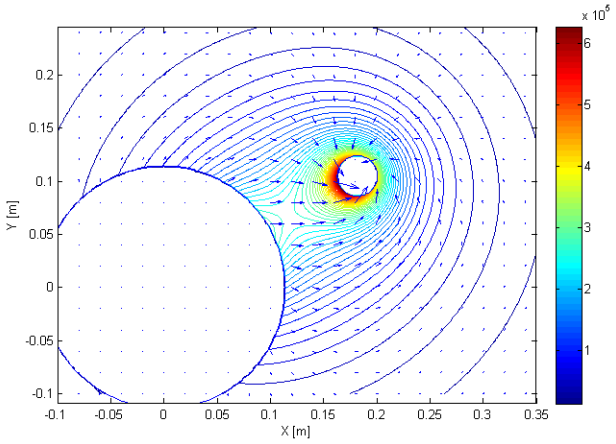

Figure 5: Analytic electric field model, used in run-time computations.

We remark that such analytic model is approximate, and it does not consider the three-dimensional effect of decaying at the sides of the cylinder. For comparison, we performed also a PDE simulation of the electric field using a 3D FEA software, as in Figure 6, and the result is close to the analytical model, at least for the zone of interest.

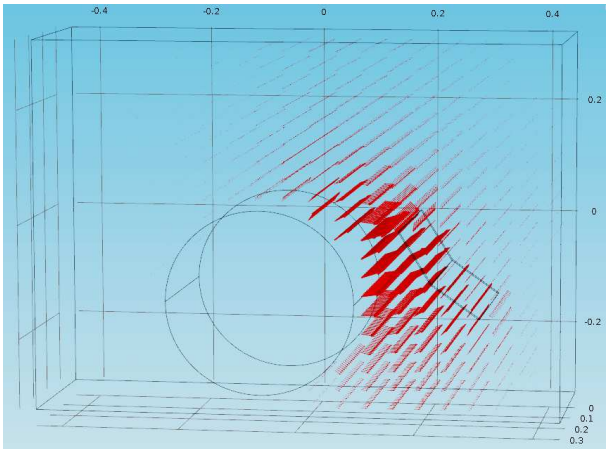

Figure 6: Reference force field, computed with PDE in off-line.

For the sake of brevity, we do not report the formulas for the aereodinamycal drag and for the gravity force, and we focus on forces caused by the electrostatic field. We make the simplifying assumptions that the metal particles discharge instantly as soon as they touch the grounded cylinder, and that charging of the non-metal particles happens instantly as soon they enter the volume in front of the cylinder.

 ISBN: 978-1-61208-371-1

We introduce the vacuum permeability ϵ_0, the relative permeability ϵ_r, the average radius of the particle r. Following [2], the force caused by the electric field acting on metallic particles is:

$$\boldsymbol{f}_{el,j} = 0.832 Q_{\text{metal}} \boldsymbol{E}(x,y,z) \tag{10}$$

where the charge Q_{metal} is

$$Q_{\text{metal}} = \frac{2}{3}\pi^3 \epsilon_0 \epsilon_r r^2 E \tag{11}$$

The non-metal particles are subject to the electric image force:

$$\boldsymbol{f}_{im,j} = \frac{Q^2_{\text{non-metal}}}{4\pi\epsilon_0\epsilon_r(2r)^2} \tag{12}$$

$$Q_{\text{non-metal}} = 3\pi\epsilon_0(2r)^2 E \frac{\epsilon_r}{\epsilon_r + 2} \tag{13}$$

We generate shapes with different densities and different sizes r and different values of ϵ_0 according to a random distribution generator, for instance one can generate flows with 30% of copper particles and 60% of plastic particles, with sizing given by probability distributions. For cases of particles made of microscopic clusters of not-separated materials, we simply apply a weighted average of the forces described above.

VI. Software implementation

The simulation software is implemented in C++ language and uses our Chrono::Engine C++ simulation libraries [25], which implement the DVI method.

To avoid the burden of defining coordinates, sizes and shapes of the collision surfaces, as well motors and joints of the CES machine, we developed a custom add-in in C# language for the SolidWorks software. The add-in allows the designer to model the system with the GUI, as in Figure 7; then one can export the environment into a file that is load and parsed by the simulator before running the simulation. On the other hand, the generation of the particle flow and the simulation loop is controlled directly by C++ statements in the stand-alone simulator, as in Figure 8.

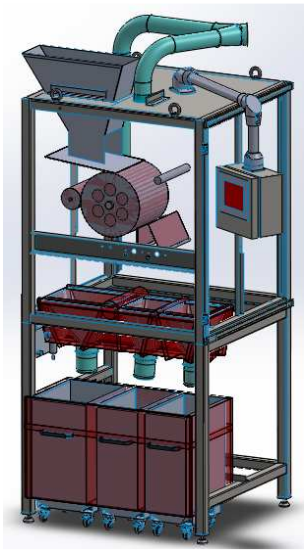

Figure 7: Model of the CES device in the SolidWork parametric CAD. Note that the surfaces that can affect collision detection have been marked as red.

Figure 8: Model of the CES device during the simulation in the OpenGL view of our Chrono::Engine software.

Post-processing of the data is performed via ad-hoc Matlab programs, although the simulator also offers an interactive OpenGL view that can be used to quickly evaluate the results of simulation tests. For the final simulations we use timesteps of 0.001 s, and the number of iterations for the solution of the CCP problem has been limited to 100.

VII. Results

Simulations can be run for different speeds of the drum, for different flow rates, and for different mixtures and size distributions of particles. At each simulation run, particle trajectories are processed by sorting their end point in virtual bins; by splitting the horizontal X direction in evenly spaced bins and by counting the particles that end into such bins, one can build statistical distributions of the output flow, as shown in Figure 9. This can be used to simulate different scenarios of operation of the CES device, and it can be used also to design new versions of the device that could process more material without incurring into inefficiency.

For instance, results in Figures 10 show how the distribution of the outcome, for the same material, increases in variance as the flow rate increases. The reason is that for high

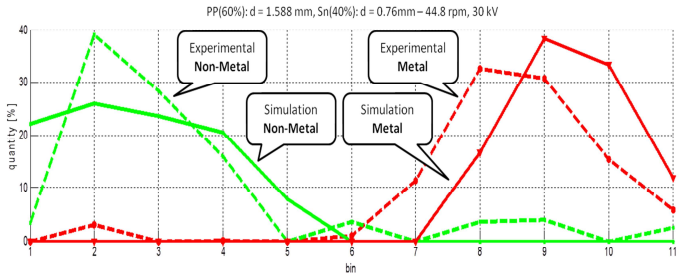

Figure 9: Output distribution showing the separation of metal and plastic particles.

flow rate the granular packing starts to be denser, as particles are more likely to be in contact each other, even in stacked layers over the drum, and this introduces more randomness in the process.

VIII. Conclusion and Future Work

We implemented a custom software, based on our Chrono::Engine simulation middleware, that can perform simulations of granular flows of particles in waste-processing devices. In detail, a CES device has been studied with this tool. The simulation method, being based on an original DVI formulation, permits large timesteps without incurring in numerical instability. Special optimizations have been used in the collision detection algorithms in order to reduce the computational overhead. A custom add-in for the SolidWorks software has been used in order to simplify the workflow, as the user can export collision shapes from the user interface of the CAD.

Future development will address experimental validation and other types of waste processing machines such as the Eddy Current Separator (ECS).

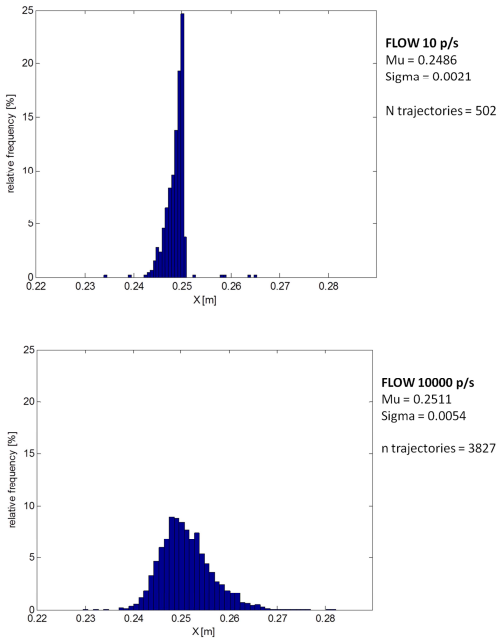

Figure 10: Output distribution of falling particles, for different flow rates.

References

[1] J. Li, Z. Xu, and Y. Zhou, “Application of corona discharge and electrostatic force to separate metals and nonmetals from crushed particles of waste printed circuit boards,” Journal of Electrostatics, vol. 65(4), 2007, pp. 233 – 238.

[2] J. Li, H. Lu, Z. Xu, and Y. Zhou, “A model for computing the trajectories of the conducting particles from waste printed circuit boards in corona electrostatic separators,” Journal of Hazardous Materials, vol. 151, no. 1, 2008, pp. 52 – 57.

[3] H. Lu, J. Li, J. Guo, and Z. Xu, “Movement behavior in electrostatic separation: Recycling of metal materials from waste printed circuit board,” Journal of Materials Processing Technology, vol. 197, no. 13, 2008, pp. 101 – 108.

[4] P. A. Cundall and O. D. L. Strack, “A discrete numerical model for granular assemblies,” Geotechnique, vol. 29, no. 1, 1979, pp. 47–65.

[5] E. Hairer, S. P. Nørsett, and G. Wanner, Solving Ordinary Differential Equations. Springer, 2010.

[6] A. Tasora and M. Anitescu, “A convex complementarity approach for simulating large granular flows,” Journal of Computational and Nonlinear Dynamics, vol. 5, no. 3, 2010, pp. 1–10.

[7] J. J. Moreau, “Standard inelastic shocks and the dynamics of unilateral constraints,” in Unilateral Problems in Structural Analysis, G. D. Piero, F. Macieri, and S. Verlag, Eds. New York: CISM Courses and Lectures no. 288, 1983, pp. 173–221.

[8] ——, “Unilateral contact and dry friction in finite freedom dynamics,” in Nonsmooth Mechanics and Applications, J. J. Moreau and P. D. Panagiotopoulos, Eds. Berlin: Springer-Verlag, 1988, pp. 1–82.

[9] F. Pfeiffer and C. Glocker, Multibody Dynamics with Unilateral Contacts. New York City: John Wiley, 1996.

[10] D. Kinderleher and G. Stampacchia, An Introduction to Variational Inequalities and Their Application. Academic Press, New York, 1980.

[11] D. E. Stewart, “Reformulations of measure differential inclusions and their closed graph property,” Journal of Differential Equations, vol. 175, 2001, pp. 108–129.

[12] D. Stewart and J.-S. Pang, “Differential variational inequalities,” Mathematical Programming, vol. 113, no. 2, 2008, pp. 345–424.

[13] D. E. Stewart and J. C. Trinkle, “An implicit time-stepping scheme for rigid-body dynamics with inelastic collisions and Coulomb friction,” International Journal for Numerical Methods in Engineering, vol. 39, 1996, pp. 2673–2691.

[14] M. Anitescu, F. A. Potra, and D. Stewart, “Time-stepping for three-dimensional rigid-body dynamics,” Computer Methods in Applied Mechanics and Engineering, vol. 177, 1999, pp. 183–197.

[15] F. Jourdan, P. Alart, and M. Jean, “A Gauss Seidel like algorithm to solve frictional contract problems,” Computer methods in applied mechanics and engineering, vol. 155, 1998, pp. 31 –47.

[16] C. A. de Coulomb, Théorie des machines simples en ayant égard au frottement de leurs parties et à la roideur des cordages. Bachelier, Paris, 1821.

[17] A. Iserles, H. Z. Munthe-Kaas, S. P. Nrsett, and A. Zanna, “Lie-group methods,” Acta Numerica, vol. 9, 2000, pp. 215–365.

[18] A. Tasora and M. Anitescu, “A matrix-free cone complementarity approach for solving large-scale, nonsmooth, rigid body dynamics,” Computer Methods in Applied Mechanics and Engineering, vol. 200, no. 5-8, 2011, pp. 439 – 453.

[19] F. Facchinei and J. Pang, Finite-dimensional variational inequalities and complementarity problems. Springer Verlag, 2003, vol. 1.

[20] M. Anitescu and A. Tasora, “An iterative approach for cone complementarity problems for nonsmooth dynamics,” Computational Optimization and Applications, vol. 47(2), 2010, pp. 207–235.

[21] E. G. Birgin, J. M. Martínez, and M. Raydan, “Nonmonotone spectral projected gradient methods on convex sets,” SIAM J. on Optimization, vol. 10, August 1999, pp. 1196–1211.

[22] E. Coumans. http://bulletphysics.org. [Online]. Available: http://BulletPhysics.org (August 2014)

[23] S. K. E.G. Gilbert, D.W. Johnson, “A fast procedure for computing the distance between complex objects in three-dimensional space,” Robotics and Automation, vol. 4, no. 2, 1988, pp. 193–203.

[24] D. Negrut, A. Tasora, H. Mazhar, T. Heyn, and P. Hahn, “Leveraging parallel computing in multibody dynamics,” Multibody System Dynamics, vol. 27, 2012, pp. 95–117, 10.1007/s11044-011-9262-y.

[25] A. Tasora. Chrono::Engine project, web page. [Online]. Available: www.chronoengine.info (August 2014)

 ISBN: 978-1-61208-371-1